Composite Structures 248 (2020) 112502

Contents lists available at ScienceDirect

Composite Structures

journal homepage: www.elsevier.com/locate/compstruct

Corner impact and compression after impact (CAI) of thin-walled composite profile – An experimental study

A. Gliszczynski [a,*], R. Bogenfeld [b], R. Degenhardt [b], T. Kubiak [a]

[a] Lodz University of Technology, Department of Strength of Materials, Stefanowskiego 1/15, 90-924 Lodz, Poland
[b] DLR, Institute of Composite Structures and Adaptive Systems, Lilienthalplatz 7, 38108 Braunschweig, Germany

ARTICLE INFO

Keywords:
Laminates
Buckling
Damage tolerance
Impact behavior
Compression after impact (CAI)

ABSTRACT

Experimental investigations of channel-section profiles subjected to compression after impacts (20 J and 30 J) leading to global failure are presented. The columns under discussion were made of an eight-layer GFRP laminate with quasi-isotropic, quasi-orthotropic and angle ply arrangements of layers. The profiles were impacted in the corner in three variants: perpendicularly to the flange, at an angle of 45 to the web and perpendicularly to the web. All impact cases were characterized by a high level of absorbed energy (over 75%), which led to a barely visible impact damage, extensive fiber rupture, visible cracks in the laminate or material continuity loss. The load carrying capacity of the profiles degraded by the corner impact always decreases in relation to the not-impacted structures but every case was characterized by stable, postbuckling equilibrium paths. The most dangerous scenario was the corner impact introduced perpendicular to the web.

1. Introduction

Nowadays different composite structures are very popular in many branches of industry like aircraft industry [1,2], aerospace engineering [3], automotive industry [4] or civil engineering [5,6]. In the literature one can find many papers dealing exclusively with the problem of impact [7–10] and those related mainly to the stability of thin-walled structures [11–14]. In vast majority of published papers, the assessment the compression after impact (CAI) strength is carried out on standardized samples [15,16] and mainly concerning the estimation of the cross-sectional strength reduction of the laminate [17–20]. Studies dealing with the impact of thin-walled structures are mainly devoted to the determination of energy absorbing characteristics such as mean force, peak force, energy absorption and crash force efficiency [21–23] or the optimization of the cross-sectional shape to maximize the crashworthiness of thin-walled structure under axial impact load [24].

However, it can also be found papers on the analysis of the phenomenon of impact and stability of structural elements. Li and Chen [25] investigated the effect of low velocity edge impact damage on the damage tolerance of wing relevant composite panels stiffened with both T- and I-shaped stiffeners under uniaxial compression load. It was found out that the presence of impact damage on the stiffener edge is more severe skin damage. Damage caused by skin impacts for equal or even higher impact energies had negligible influence on the residual strength. In addition, it was highlighted that under identical edge impact levels, the damage tolerance behavior of T-stiffened composite panel is distinctly superior to that of I-stiffened composite panel, which results in more cautious design regarding edge impact damage tolerance of the panel stiffened with I-stiffeners. Greenhalgh et al. [26,27] analyzed panels containing inclusions introduced during fabrication and impact damage under monotonic compression loading. It was stated that the presence of defects led to a reduction in the strength ranging from 7% (bay impact) to 29% (foot impact). Nevertheless, the conclusion was that modelling impact damage as a single plane embedded defect is of limited validity and may be non-conservative. Kootte and Bisagni [28] presented a methodology to investigate and improve the strength and damage tolerance of stiffened composite panels used in aerospace structures subjected to postbuckling deformation. Dávila and Bisagni [29] investigated the fatigue life and damage tolerance of composite stiffened panels with indentation damage. The authors presented the superiority of indentation to impact studies paying attention to the simplicity of application, less dependence on boundary conditions, better controllability, and repeatability of the imparted damage. The approach proposed by the authors enabled a comparison of different tests and the potential identification of the effects that influence the fatigue lives and damage

* Corresponding author.
E-mail addresses: adrian.gliszczynski@p.lodz.pl (A. Gliszczynski), raffael.bogenfeld@dlr.de (R. Bogenfeld), richard.degenhardt@dlr.de (R. Degenhardt), tomasz.kubiak@p.lodz.pl (T. Kubiak).

https://doi.org/10.1016/j.compstruct.2020.112502
Received 10 March 2020; Accepted 19 May 2020
Available online 28 May 2020

tolerance of postbuckled structures with defects. Wang et al. [30] conducted the experimental investigation on stiffened composite panels with predamage implemented at the vulnerable stiffener edge. Experimental analysis indicated that the outer sublaminate at the damage location was buckled before the global buckling occurred. The post-failure analysis confirmed that the multiple delaminations and the unstable buckling took place at the damage site firstly and propagate transversely.

The literature cited, however, lacks papers on the behavior of elements from the border of coupon and structural level. Thus, the authors of this manuscript decided to analyze the thin walled profile, which geometrically is not as simple as standard specimen and not as advanced as stringer-stiffened panels. In the context of the research undertaken, one can distinguish the Kubiak et al. [31], who analyzed bending after impact of thin-walled channel section profiles. The authors analyzed low velocity impacts introduced in the middle of the flange and the web widths but the obtained results indicated the conclusion that the impact damages have no significant influence on the behavior of channel section profiles during the bending tests.

The research that underlies this article is a continuation of the experimental tests conducted on pre-degraded thin-walled profiles [32,33]. Previous studies of the authors have shown that the impact on the flange and the web has no significant effect on the reduction of buckling and load carrying capacity load [32], while impacts around the corners, carried out for similar profiles made of GFRP but characterized by over twice smaller thickness, led to almost two-fold reduction of the load capacity in relation to reference structures (not impacted) [33]. However, in [33], due to the risk of the impactor slipping and the risk of permanent damage to the impact testing machine, the authors shifted the impact axis of the impactor by half the impactor diameter towards the longitudinal plane of symmetry of the profile. In the presented research, the use of a portable impact device (Gas Gun) allowed the introduction of impacts exactly at the corners of the considered channel section columns. In the undertaken research, care was taken not only to introduce the impact exactly into the corner of the C-shaped columns, but also to examine the angular position of the impactor on the nature of the generated damages and their influence on pre- and postbuckling behavior during compression after impact test. In addition, in contrast to [32], in this paper not only 20 J but 30 J of impact energy was considered, which in the case of impact tests on the standardized plates [15], made of the same material and layer systems, led to the formation of barely visible impact damages – BVIDs (20 J) or partial material perforation (30 J), respectively [34].

According to the theory of elastic stability proves that thin-walled plate systems subjected to compression, after reaching the buckling load and loss of stability in the elastic range, are able to transmit the load in postbuckling range [35,36]. The tests carried out assumed that the impact is introduced in a place providing the tested profiles with the highest stiffness in the tested profiles – these places are the corners. Therefore, the objective of the diligently research was also to find the answer to the question whether, in case of impact degradation, a thin-walled structure will retain a stable equilibrium path in postbuckling state (if such state will in fact exist) or the post-impact damage will lead to general strength reduction of the composite and the structure will reach load carrying capacity before losing stability. Therefore, the objective of the undertaken research was also to find the answer to the question whether, in case of impact degradation, a thin-walled structure will retain a stable equilibrium path in postbuckling state (if such state will in fact exist) or the post-impact damage will lead to general strength reduction of the composite and the structure will reach load carrying capacity before losing stability.

2. Object of analysis

Thin-walled short channel section columns (Fig. 1) with cross-section dimension of $W \times H \times t = 80 \times 40 \times 2$ mm (W – the web width, H – the flange height and t – the wall thickness) manufactured using autoclaving technique were considered. The length (L) of considered profiles was equal to 250 mm. Columns were made of eight layers unidirectional GFRP laminate with a ply thickness of $t_{PLY} = 0.26$ mm and the material properties presented in Table 1. Ply elastic properties (E_1, E_2, G_{12}, ν_{12}) and ply strengths (T_1, T_2, C_1, C_2, S_{12}) were measured using test standards defined by ASTM [37,38]. The thin-walled composite profiles with channel section were made of unidirectional pre-preg band (denoted as SE70/EGL/300 g/400 mm/35%/PoPa).

The investigated columns had a quasi-isotropic (QI), quasi-orthotropic (QO) and angle ply (AP) arrangement of layers (cf. Table 2). It was assumed that the layups under consideration had their general axis of orthotropy, 0° and 90°, parallel and perpendicular to the longitudinal edges of the profiles (cf. Fig. 1).

3. Test stands

In the conducted investigations, two different test stands were applied. The first one was used to introduce impact damage and the second one to perform CAI tests.

3.1. Impact test

A scheme of the impact test stand is presented in the Fig. 1. The considered specimens were fixed on a clamped aluminum support. Possible displacement of profiles during impact was omitted using two inserts and two clamping elements pressing the profiles to the inserts. These elements were made of polyethylene (PE). The distance between the profile clamping elements (dim. A = 100 mm, cf. Fig. 1) corresponds to the width of the standard samples used for examining the phenomenon of low velocity impact [15].

In the conducted studies all impact tests were conducted using an Impact Gas Gun. A hemispherical impactor with diameter of 16 mm and the mass of $M = 0.8353$ kg was chosen for all impacts. The impact on the corner of the channel section profiles was considered in three variants: perpendicularly to the flange – 0 (Fig. 2a), at an angle of 45° to the web – 45 (Fig. 2b) and perpendicularly to the web – 90 (Fig. 2c). It should be noted that the impact position was always radial to the curvature of the corner, to avoid lateral contact forces and a slipping of the impactor. The real test stand together with the simplified denotation of the impact schemes (0, 45, 90) is shown in Fig. 2. In the 0 and 90 positions the impact gas gun was placed through an orthogonal stop bracket (Fig. 3). To conduct the angular impacts (45) the gas gun was positioned through a groove in the impact gun's barrel. The angle of 45° was manually adjusted with the help of an angular sensor mounted on the gun barrel (Fig. 3). Due to the limited number of samples made of the material previously considered in many configurations [31,32], the experimental tests were carried out with one only repetition for each of the configurations listed in Table 3.

The major advantage of impact testing with a gas gun is in the flexibility. The gas gun used for the tests is typically applied for impact tests on the structural level, where arbitrary geometrical configurations need to be impacted. Moreover, a gas gun impact also offers additional possibilities on the coupon level. With an appropriate specimen fixture, any accessible point of that specimen can be impacted under an arbitrary angle. Nonetheless, in comparison with drop tower tests the use of the gas gun entails several challenges. Firstly, the manipulated variable to achieve the specified impact energy is the charging pressure. However, there are several other influencing factors on the actual impact energy. A change of the gravitational influence (by the angle of the impact gun) or different environmental conditions require a corrective action to achieve the specified energy value. For the applied energy range in the present study, these influencing factors

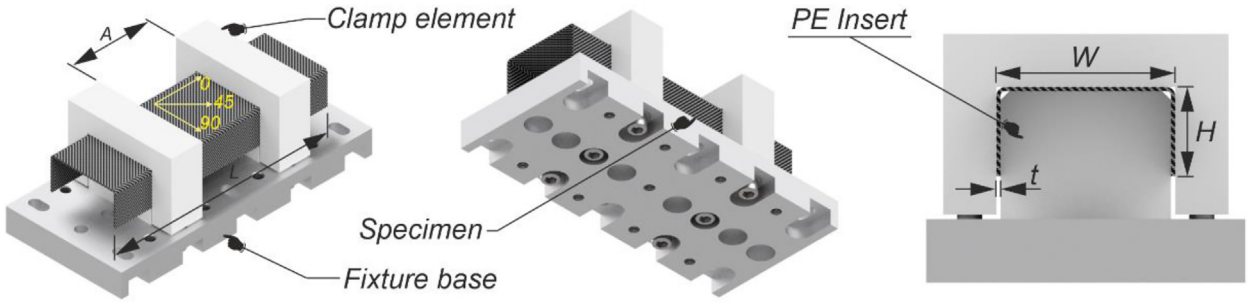

Fig. 1. Schematic impact test stand.

Table 1
Mechanical and strength properties of unidirectional glass/epoxy composite ply.

Mechanical properties	E_1 [MPa]	E_2 [MPa]	G_{12} [MPa]	v_{12} [–]	
	38 500	8100	2000	0.27	
Ply strengths	T_1 [MPa]	C_1 [MPa]	T_2 [MPa]	C_2 [MPa]	S_{12} [MPa]
	792	679	39	71	108

Table 2
Analyzed arrangements of layers and their simplified denotation.

Quasi-Isotropic	Quasi-Orthotropic	Angle-Ply
QI	QO	AP
[90/−45/45/0]s	[0/90/0/90]s	[45/−45/45/−45]s

result in an energy uncertainty of around ±1 J. To achieve a maximum level of accuracy, a calibration of the operation pressure was conducted for each impact position separately. Furthermore, all impacts were conducted in one test series under constant environmental conditions (23 °C, 50% relative humidity). The second significant challenge in conducting impacts with a gas gun is the available measurement system. The crucial metric of an impact event, the contact force, cannot be recorded. Instead, the impact gun only measures the impactor position with a relatively low sampling rate of 50 kHz. The exclusive availability of a displacement measurement is not an issue. The time derivatives of the displacement history result in the history curves for the velocity and the acceleration. The force response results directly from the latter. However, the quality of velocity and force history is insufficient as the derivation amplifies the noise of the original curve. The unfiltered raw curves are unusable so to evaluate the force history, there is an indispensable need for an appropriate filtering algorithm.

3.1.1. Data filtering

The choice of an appropriate filtering algorithm is the key to extract some informative value from the recorded data of the impact gun. A filtering algorithm for impact data has to account for several factors. Unwanted oscillation has to be removed. Effects resulting from the actual impact shall be kept as true to original as possible. The maximum contact force, sudden force drops and the following oscillation shall be kept, to assess what happened during the impact. Three filtering methods are compared for that purpose. A Savitzky Golay (SG) Fil-

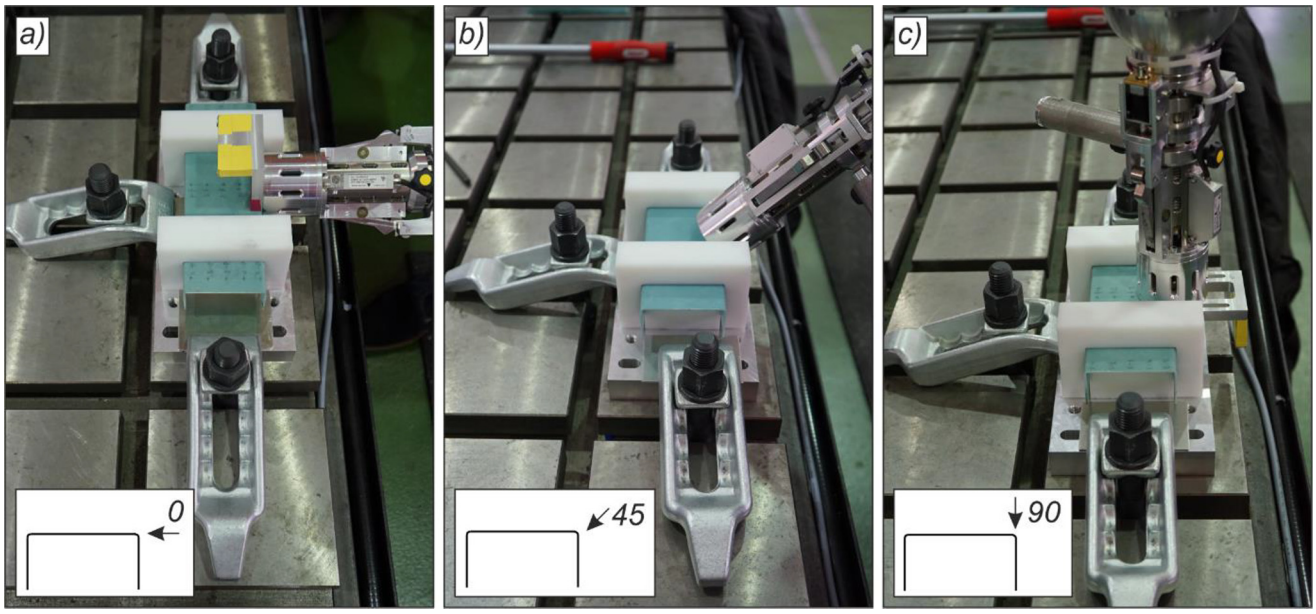

Fig. 2. Considered variants of corner impacts.

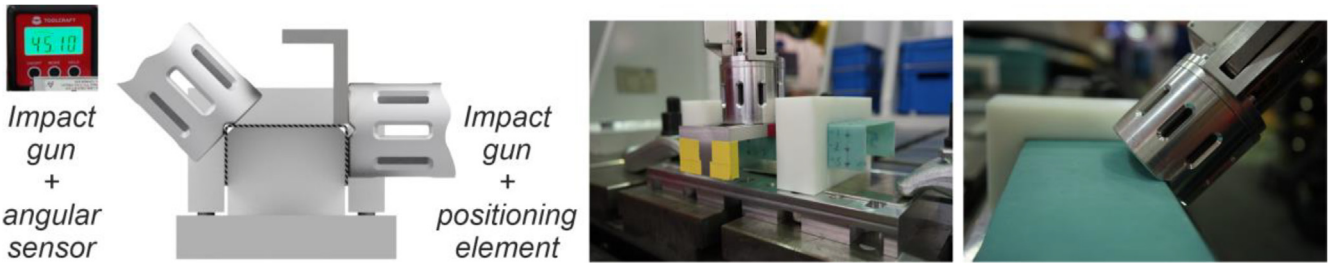

Fig. 3. Gas gun positioning scheme.

Table 3
Considered impact scenarios for the analyzed ply systems.

Impact energy	QI	QO	AP
20 J	–	0	0
	45	45	45
	–	90	90
30 J	45	45	45

ter [39], a Butterworth (BW) filter [40] and a Finite Impulse Response filter (FIR) [41]. The Fig. 4 includes the comparison of all considered filtering algorithms.

The resulting curves of all filters show a similar trend. The high-frequent oscillation induced by the noise is removed. However, a second source of disturbance becomes visible. Apparently, there is an oscillation between 1 and 1.5 kHz coming from the impact gun itself. Strong smoothing is required to achieve a force response without the influence of this higher-order vibration. The maximum cut-off frequency of the BW filter is around 1 kHz. Such a strong filter also removes any occurring force drop and all damage-caused vibrations.

The application of the FIR algorithm consisted in calculating subsequent derivatives of the impactor displacement assuming the number of averaged successive signal digital components at the level of twenty. The FIR filter removes both the noise and the artificial oscillation and the result curve has the same global trend as when processed by SG or BW filters. Nevertheless, the information about the impact process is available and force drops can be identified. For the mentioned reasons, the FIR is the method of choice to filtering the recorded impact history data in this test series.

3.2. Compression after impact test

The CAI tests were conducted on a universal testing machine (UTM) produced by Instron and modernized by Zwick-Roell (Fig. 5b). The CAI tests were carried out in the form of uniform shortening of the profiles to the global failure of the columns. The velocity of the traverse was set to 1 mm/min. A scheme of the performed compression test is presented in Fig. 5a. The upper plate as well as the bottom table on the test stand had milled grooves (Fig. 5c) with the shape corresponding to the investigated cross-section.

The loading force and the displacement of the upper jaw of the machine were collected directly from the UTM sensors. To determine deflections of the columns in the whole range of load, a Digital Image Correlation (DIC) system (Aramis) was employed. The data from the

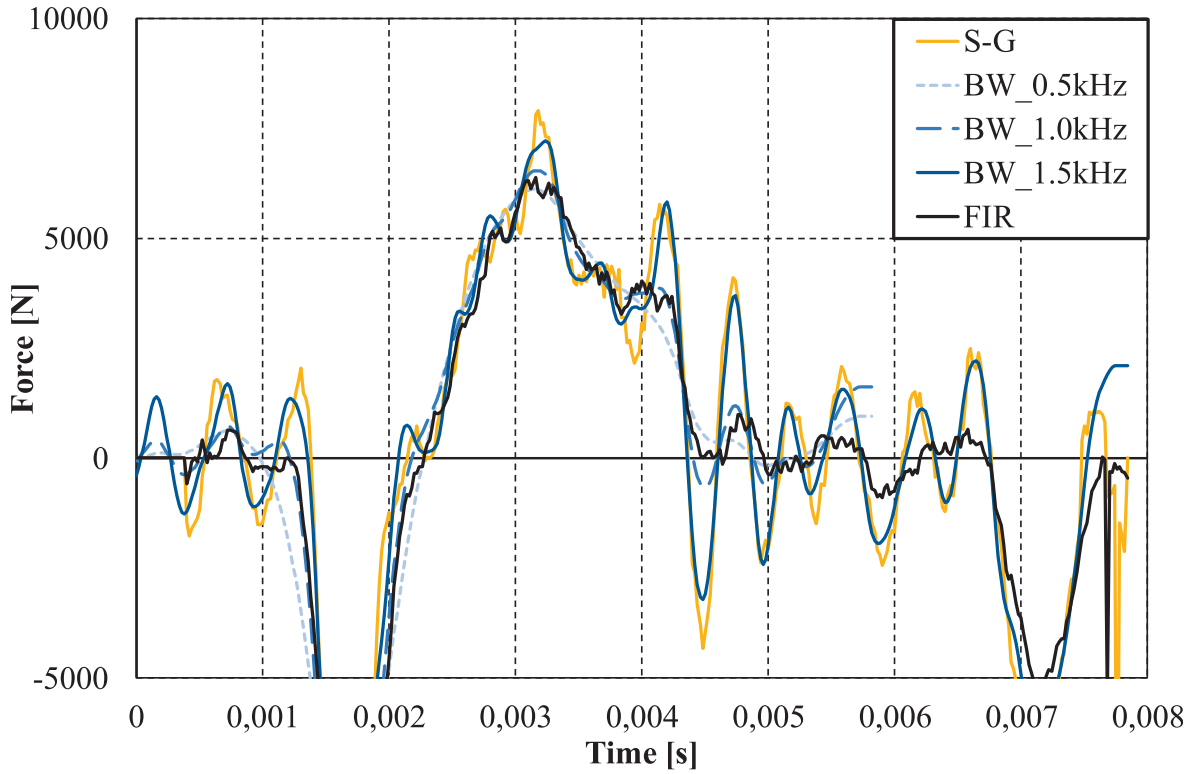

Fig. 4. Influence of using various data filtering algorithms.

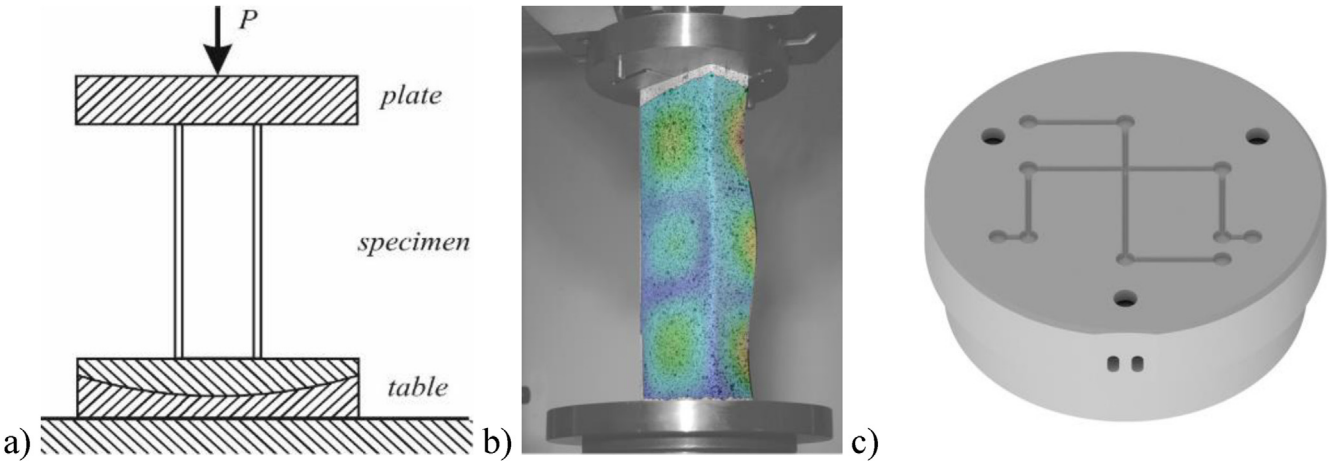

Fig. 5. The scheme (a) and the real test stand (b) for compression test with milled grooves (c).

DIC was captured with a frequency of 1 Hz together with load transferred directly from the testing machine. More details about the experimental procedure and the equipment used can be found in Gliszczynski et al. [32], Kubiak et al. [33] or Urbaniak et al. [42] papers. In the context of CAI tests, the paper presents the reference results of structures nonimpacted and degraded by the impact introduced into the web and the flange [32]. It is mentioned that the QI, QO and AP systems correspond in the paper [32] with the C2, C4 and C5 ply systems, respectively.

4. Ultrasonic evaluation

To determine the damage areas and preliminarily identify damage forms of channel section columns, non-destructive ultrasonic tests (UT) were performed. The tests in an immersion tank with a Olympus V309 ultrasonic transducer with a 5 MHz frequency, a focal length of 50 mm, and a width of 0,5 in. The scanning of the channel section columns comprised the evaluation of the sound level reduction of the backwall echo (C-Scan) and the time of flight evaluation of the pulse echo (D-Scan). While the C-Scan technique provides reliable information about the damage envelope the D-Scan permits the allocation of the delamination damage to a particular ply interface in the laminate.

Due to the curvature of the corners of the tested channel section profiles and the lack of an appropriate measuring equipment, allowing for ultrasound assessment in this area, it was decided to combine two flat ultrasonic C-scans (flange and web) with photo of the degraded corners (cf. Fig. 6) for each specimen. In this way, a developed view, covering the surfaces of the flange, web and corner seen from the impact side, was prepared. Due to the size of the prepared combinations, the projection of damages in the remaining analyzed cases was reduced only to *Detailed area*-s (cf. Fig. 6).

5. Results and discussion

First, an influence of the impact angle and the arrangement of layers on the areas and types of occurring damages was investigated. The

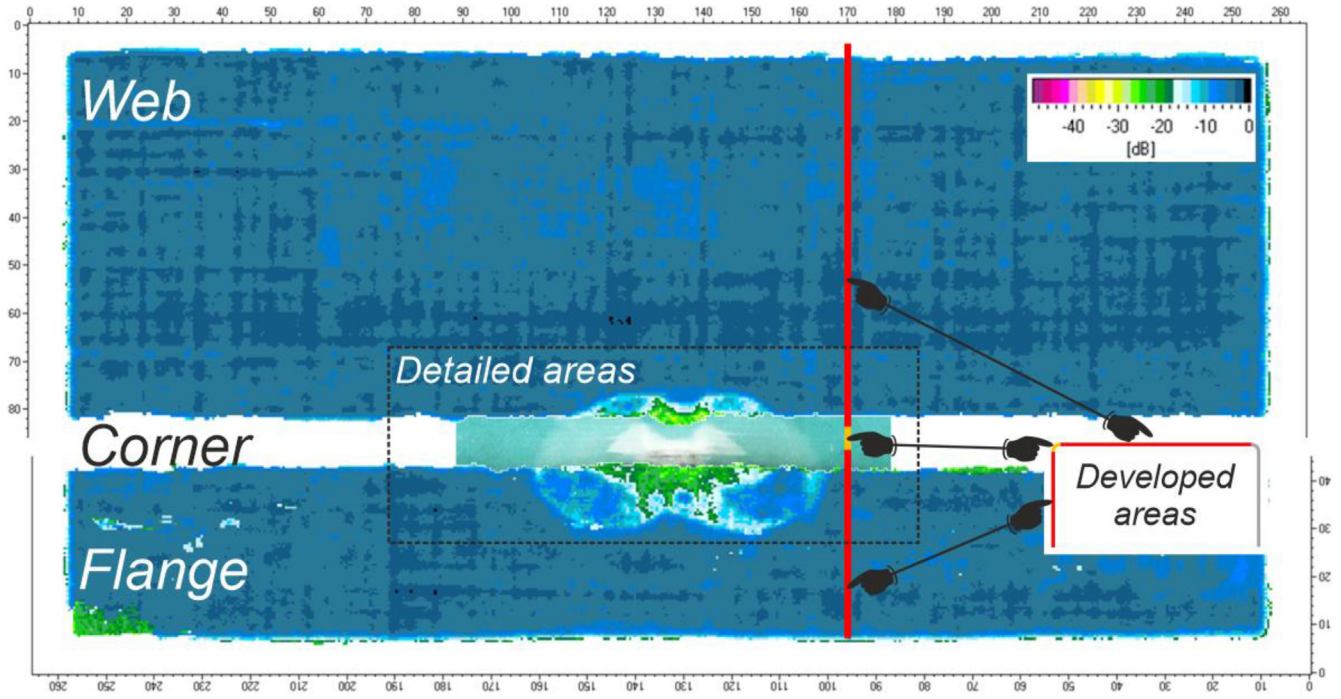

Fig. 6. An exemplary combination of ultrasonic C-scans and a photo used to measure the damage area in the developed view.

next step of the analysis was the evaluation of stability and load carrying capacity of the investigated structures from CAI tests.

5.1. Impact analysis

In accordance with the presented data filtering procedure using a two-stage FIR filter (Section 3.1.1.), force-time histories (Fig. 7) and characteristic values of impact parameters, such as: E_M – maximum energy measured during the impact test, E_{ABS} – absorbed energy, F_{MAX} – maximum contact force, u_{MAX} – maximum registered indentation and t_{IMP} –imapct time, were determined.

At the outset, it should be noted that the differences between the nominal and measured impact energy resulted directly from the principle of the gas gun operation. Although the gas-gun was subjected to a calibration process for each considered angular position (0, 45, 90), the changing charge pressure caused different values of effective impact energy, with the differences in none of the analyzed cases exceeding 2 J.

The results included in the Table 4 and Fig. 7 reveal that the quasi-isotropic system was characterized by the highest stiffness and contact force. In other cases, there is no constant correlation between the impact angle and the maximum force recorded during the impact. The results of ultrasonic examinations, presented in the Fig. 8, allowed to determine the projected delamination areas.

Traditionally, the increase of the impact energy corresponded to the increase of the recorded damage areas. However, it was also noted that the impact perpendicular to the web (90) generated the largest areas of damage. In the context of the analysis of ply systems, the damage in the quasi-orthotropic stacking is comparable to that of standardized impact samples [43,44], characterized by a peanut shape. This observation is remarkable due to the significant differences in relation to the impact setup itself compared to standard research on the impact influence to flat [21] or homogeneously curved laminates [45]. The damage in the other two laminate cases is characterized by a compact damage distribution.

According to the current state of the art, the damage categorization in the scope of applicability of BVIDs [46] usually consists of measuring permanent indentation just after the impact test. The measurement of such a characteristic parameter is most often carried out in the case of LVI tests of standardized composite plates [15] or shells with a significant radius of curvature [47]. Moreover, depending on the impact angle, different limit values of the permanent indentation should be determined. Therefore, in order to categorize the damage, the results of ultrasound examinations were supplemented with macroscopic observations. Due to the transparency of the material under consideration, a strong light source allowed the determination of damage projection almost identical to the results of ultrasound tests. The combination of both approaches allowed the categorization of observed damage into the following 4 categories: *BVID* – barely visible impact damage, *FT* – Extensive Fiber Rupture, *CRACK* – visible crack of laminate and *MCL* – material continuity loss. The intention of the authors was that each subsequent level of damage contains the previous pattern of damage. Thus, *FT* should be understood as *BVID* with a larger percentage of damaged reinforcing fibers, located mainly on the side opposite to the impact. *CRACK* means a state in which fiber breakage was visible on both sides of the laminate but it did not generate significant differences in the shape of the profile compared to the state prior to the impact. The loss of continuity referred to the creation of permanent indentation at the impact site, which was certainly the result of massive fiber cracking on both sides of the laminate. In addition, it should be mentioned that the ultrasound examinations of the web and the flange reveal a decrease of the signal amplitude close to the specimen corner. However, an accurate analysis of the C-scans allows stating that only in the case of the quasi-isotropic system, the impacts caused a damage-relevant stress wave propagation outside the area limited by the two clamps and inserts. The respective damage formation is visible in the form of two longitudinal delaminations along the corners of the considered profiles (Fig. 9d), which corresponded to a decrease in signal amplitude close to the corner.

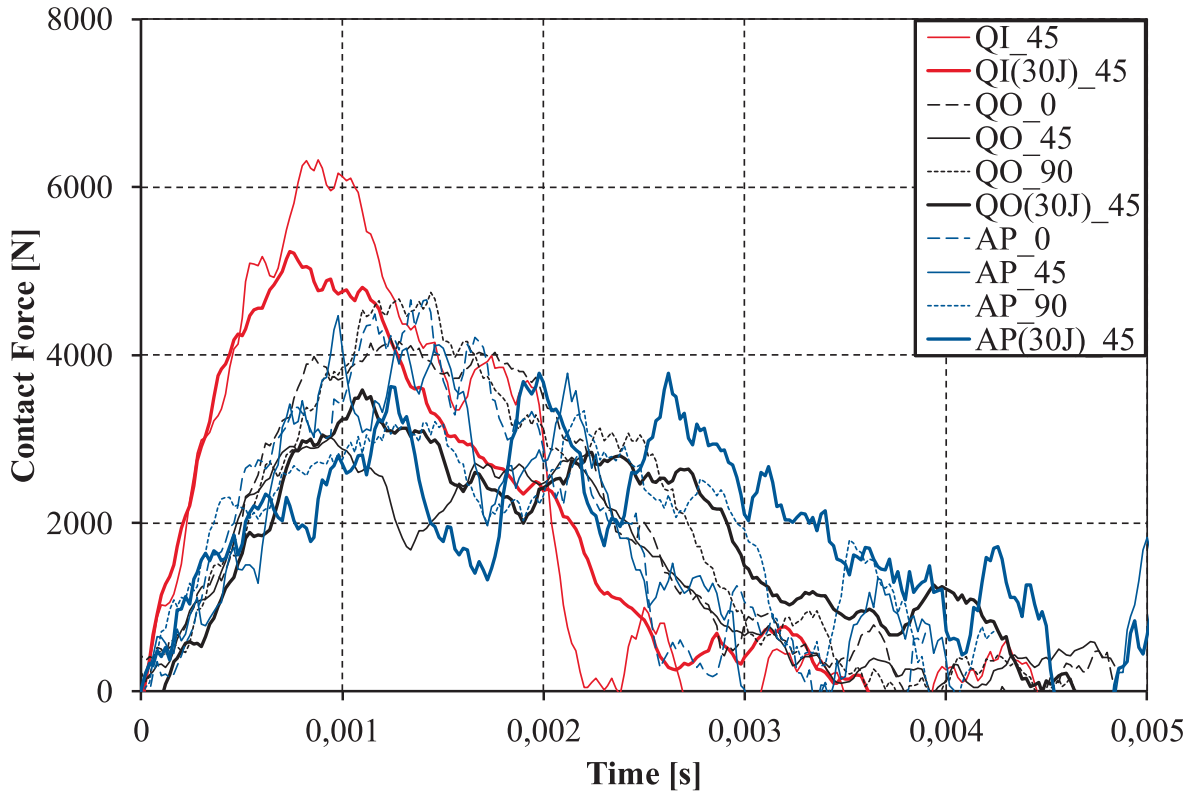

Fig. 7. Force – time histories of the conducted impact tests.

Table 4
Characteristic parameters of impact tests.

Ply system	Impact energy	Impact angle	E_M [J]	E_{ABS} [J]	F_{MAX} [kN]	u_{MAX} [mm]	t_{IMP} [ms]	A_{DEL} [mm^2]
QI	20 J	45	21,2	16,9	6,48	4,1	2,4	505
	30 J	45	30,3	28,6	5,76	7,0	2,8	754
QO	20 J	0	20,0	15,8	4,36	6,5	3,1	972
		45	20,9	20,5	3,35	9,3	4,0	859
		90	21,7	16,3	4,80	9,1	3,6	1045
	30 J	45	30,6	29,5	3,66	12,0	4,5	1432
AP	20 J	0	19,8	17,6	4,29	7,3	2,4	684
		45	21,3	20,5	3,77	9,7	3,1	641
		90	22,0	18,4	3,05	8,9	4,1	918
	30 J	45	30,0	26,9	3,05	14,2	4,8	1152

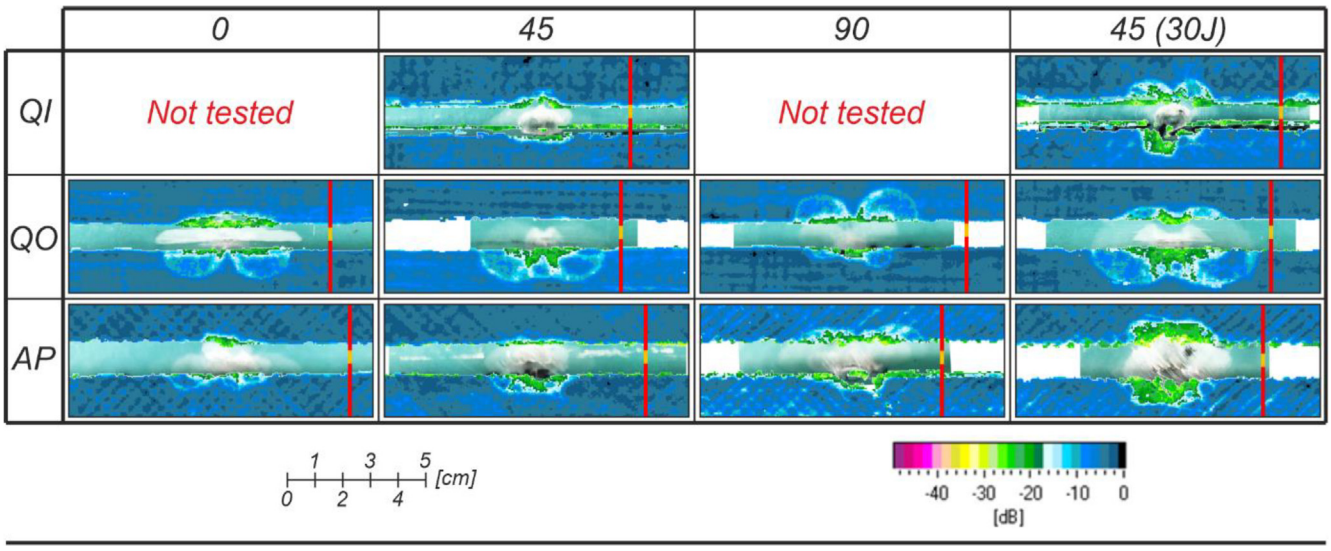

Fig. 8. Detailed areas of corner impact damages.

In the case of thin laminates [48–50] the simplified distribution of BVIDs corresponds to pine tree pattern [51], in which the largest degradation is observed on the opposite side of the impact. In case of BVIDs, the presence of numerous delaminations between successive layers of the laminate and areas of the damaged matrix within which individual fiber rupture is assumed. An example of the BVIDs distribution is presented on the Figs. 9c and 10. It is noteworthy that in standardized rectangular plates used for cross-sectional strength reduction of fiber laminate [34], the absorption energy generally does not exceed 50% of the nominal impact energy [10,19,20] while in the case of the tested plate systems the lowest absorption energy represented for nearly 75% of nominal energy. It should be remembered, however, that the boundary conditions in which a standard impact test is carried out [15] are drastically different from those adopted in the context of the tests performed. In the case of the conducted impact tests, BVIDs were observed only in few cases of a quasi-isotropic and quasi-orthotropic profiles impacted with energy of 20 J.

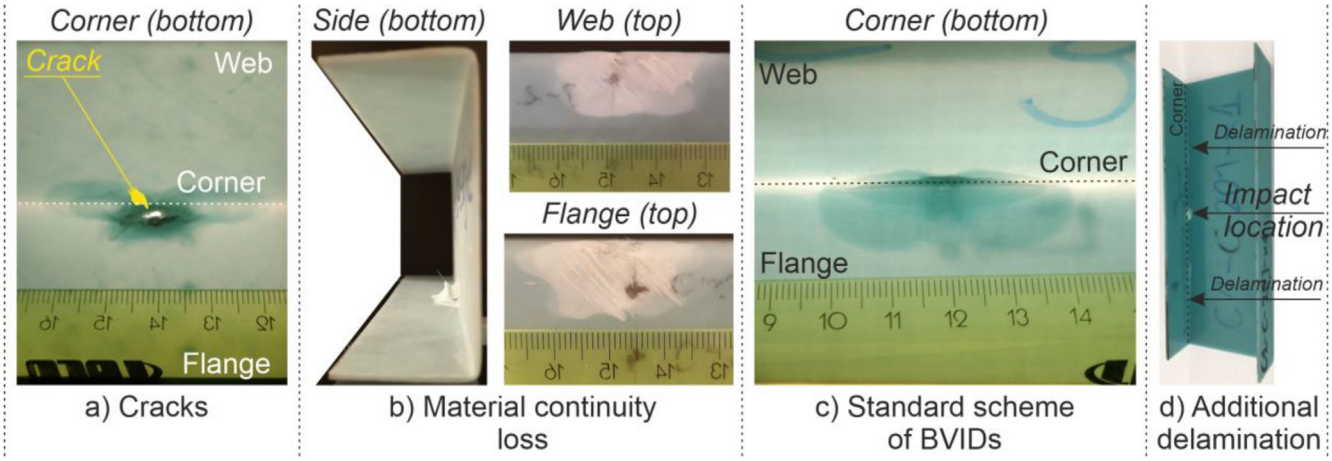

Fig. 9. Characteristic types of observed damages.

Analyzing the data from the Table 4, it can also be seen that in the case of 20 J impacts, the absorbed energies, within a specific layer system, have similar values, although the maximum always occurred in case of the angular impact (45). Impacts at an angle of 45 degrees are not only characterized by the highest energy absorption but also the largest registered indentation and at the same time the relatively smallest area of damage in relation to both other considered impact positions (0, 90). In addition, in cases of 20 J impacts, regardless of the angular position of the impactor, the quasi-orthotropic system is characterized by lower energy absorption than the angle ply system. Due to the higher stiffness in the quasi-orthotropic laminates, larger areas of projected damages emerge for this ply system while maintaining an almost identical maximum indentation as the angle ply system.

In the context of 30 J impacts, the absorbed energy values exceed 90% of the nominal impact energy. It is not surprising then that these cases were characterized by the largest areas of damage. With regard to the quasi-isotropic and quasi-orthotropic system, 30 J impacts generated a BVID-like damage pattern, in which however the rupture of the reinforcing fibers played a dominant role - FR. However, the corner geometry did not change significantly.

Different types of damage were revealed for the angle ply system, in which the dominant types of damage were the loss of material continuity (on the opposite side to the impact) or the presence of a visible laminate crack (cf. Table 5, Fig. 9a and b). The authors would like to mention, however, that in the case of the angle ply system impacted perpendicularly to the web (90) with an energy of 20 J, macroscopic analysis allow to conclude that the reinforcing fibers have cracked through all layers (visible gap). However, in the case of an impact perpendicular to the flange (0), cracks on the impact and the opposite side can be noticed, but the overexposure of the damage area does not allow to determine whether the crack passes through the entire thickness of the laminate (Crack *).

The maximum forces recorded during the 30 J impacts most often did not exceed the values recorded at 20 J of impact energy (cf. Table 4). Hence, the impact energy of 20 J was already sufficient to exceed the critical force threshold at which major damages occurs and limits the laminate capacity to bear transversal load [52]. Nonetheless, the damage extent further increases after this threshold force is exceeded. This can be observed, taking into account the much more severe pattern of introduced material degradations and much higher indentation during the impact test. The smaller maximum force recorded during the test is understandable and in line with the results included in the paper by Gliszczynski et al. [34].

5.2. Compression after impact analysis

CAI tests allowed to determine buckling and collapse modes as well as load carrying capacities and failure loads of considered structures. The figures summarizing the tests carried out were supplemented with

Table 5
Major type of observed damages.

Ply system	Impact energy	Impact angle	Damage type
QI	20 J	45	BVID
	30 J	45	FR
QO	20 J	0	BVID
		45	BVID
		90	BVID/FR
	30 J	45	FR
AP	20 J	0	CRACK*
		45	CL
		90	CRACK
	30 J	45	CL

reference results for non-degraded structures (*REF.*) and compression tests of analogous columns impacted at different locations relative to their height (mid-span (*1/2*) or one-third of the column's height (*1/3*)) in the middles of the flange (*FLANGE*) or web (*WEB*)) [32]. The load-shortening curves, representing the global response of the considered profiles, were presented in the Fig. 11. Characteristic points of the Fig. 11a-c, such as: load carrying capacity (P_{MAX}), maximum shortening corresponding to achieving maximum compressive force (δ_{MAX}), failure load (P_{FAIL}) corresponding to a sudden decrease in compressive force and the corresponding shortening (δ_{FAIL}) are summarized in Table 6. An exemplary, graphical interpretation of these parameters is shown in the Fig. 11c (data series: *AP_Corner_90* and *AP_REF.*). It is mentioned that the *K* parameter refers to the stiffness of the tested systems and was determined in the prebuckling state from force-shortening curves from 2 to 5 kN.

Based on the results of the conducted research, it can be concluded that the load capacity of the channel section profiles degraded by the corner impacts always decreases in relation to the reference (nonimpacted) structures. Such a constant relationship was not observed in cases of analogous structures impacted on the web or the flange removed from the corner [32]. In addition, it is worth noting that all C-shaped columns, initially degraded by corner impacts with 20 J and 30 J energy, were characterized by stable, post-buckling equilibrium paths.

5.2.1. 20 J impacts

In the case of 20J impacts, the highest load capacity decreases were observed for the impact cases perpendicular to the web (90). These decreases were 34% and 44% for QO and AP, respectively. In other cases, the capacity decrease ranges from 14 to 38%. Regardless of the layer system considered, in cases of 20 J impact, the courses of the recorded curves do not differ significantly from the reference ones. The maximum change in the prebuckling stiffness in these cases does not exceed 8%. Therefore, while maintaining similar stiffness, it is not surprising that in each of the analyzed cases the decrease in the load

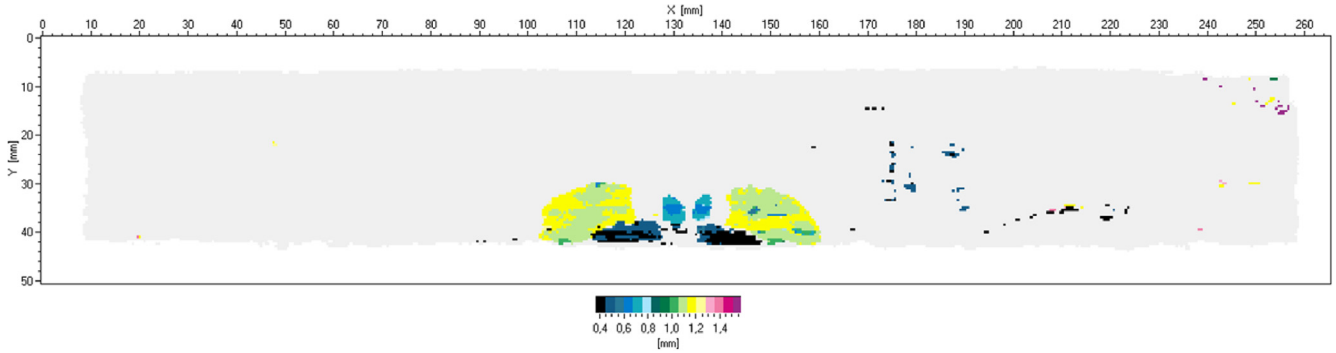

Fig. 10. An example of delamination distribution in relation to the thickness of the laminate under consideration (flange).

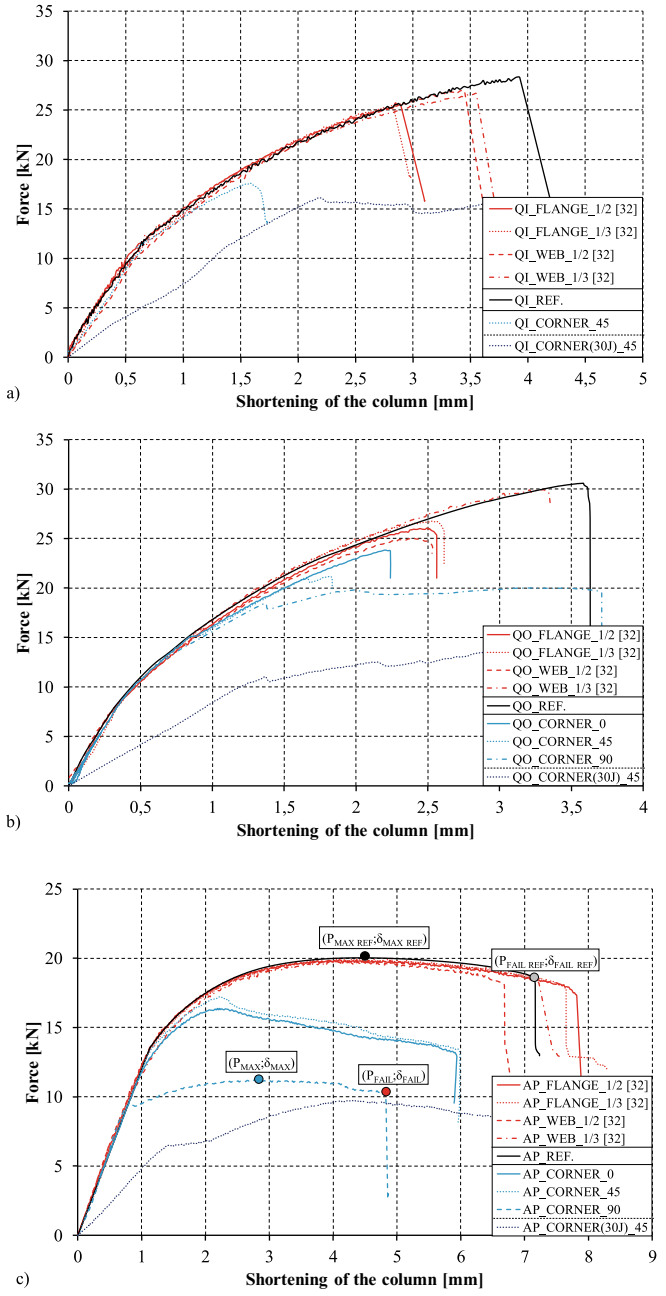

Fig. 11. Load vs shortening curves for: quasi-isotropic (a), quasi-orthotropic (b) and angle-ply columns (c).

carrying capacity is accompanied by an average of nearly two-fold decrease in shortening, corresponding to the maximum compressive force achieved by the profile ($\delta_{MAX}/\delta_{MAX\ REF}$). In the case of an angle ply system, even local loss of material continuity and material cracks did not cause significant differences in the context of the identified stiffness in the prebuckling state. In cases of 20J corner impacts perpendicular to the web (90), in both tested laminate cases (QO and AP), the initiated damage pattern reflected the state between those recorded for the other considered impact positions (0, 45) and those recorded for 30J energy (45). The CAI tests of these columns have revealed that in the lack of significant differences in stiffness, the profiles are characterized by the highest, continuous (range of almost constant compressive force with increasing shortening of the profile) load carrying capacity decrease, as is the case with the formation of plastic mechanisms. In cases of damages classified as BVID, the similarity between force-shortening curves determined for pre-degraded and reference systems is noteworthy. For quasi-isotropic and quasi-orthotropic arrangements of layers, global failure of the profile occurs almost immediately after reaching the maximum compressive force. A different process of capacity loss concerns columns with angle ply system. In these cases, reaching the maximum compressive force is not accompanied by a sudden capacity loss, but only by a curvature of the curve. Interestingly, even in the case of an impact introduced into the corner, the course of the force vs shortening curve retains similar features, i.e.: identical stiffness in the prebuckling range, a long range of slightly decreasing compressive force with increasing shortening of the profile in postbuckling range, different values of the capacity (P_{MAX}) and the force corresponding to the total failure of the profile (P_{FAIL}).

5.2.2. 30J impacts

Due to the fact that the 30J impacts led to a material continuity loss or damage areas significantly exceeding those of the BVID damage, also the obtained decrease in the load capacity reached the highest level. Regardless of the considered arrangement of layers, the load-carrying capacities of these profiles decreased to about half of the reference values. In opposition to the 20J impacts, the energy of 30J led in all analyzed cases to a significant reduction of the prebuckling stiffness. In relation to the reference results, the decrease in stiffness ranged from 60% (AP) to 70% (QO). The nature of the damage initiated by the 30J impact changes not only the prebuckling behavior but also the entire character of the recorded curves. This is most evident in the case of the quasi-isotropic and the quasi-orthotropic system, where significant ranges of almost unchanging (QI) or slowly increasing compressive force (QO) with a constantly increasing shortening were observed. For the undamaged reference case and the cases with impact damage degradation removed from the corner [32], the loss of load capacity in these cases was almost immediate after reaching the maximum compressive force. The pre-degraded channel section profiles

Table 6
Characteristic parameters of CAI tests.

Ply system	Impact energy	Impact angle	P_{MAX} [kN]	P_{FAIL} [kN]	δ_{MAX} [mm]	δ_{FAIL} [mm]	K [kN/mm]
QI	20 J	45	17,49	16,73	1,60	1,68	17,52
	30 J	45	16,11	15,92	2,19	3,98	6,35
Reference			28,30	28,30	3,92	3,92	17,30
QO	20 J	0	23,79	23,73	2,19	2,24	25,45
		45	21,15	21,03	1,80	1,83	26,45
		90	20,01	19,59	3,17	3,70	27,94
	30 J	45	14,69	14,69	3,25	3,25	8,05
Reference			30,37	29,83	3,58	3,62	26,60
AP	20 J	0	16,29	13,12	2,27	5,91	11,68
		45	17,16	13,39	2,23	5,99	12,21
		90	11,12	10,31	2,94	4,84	13,53
	30 J	45	9,69	7,94	4,32	7,21	4,98
Reference			20,02	18,3	4,42	7,16	12,50

with angle ply systems is also characterized by similar features but in this case significant differences between the load carrying capacity and the failure load (P_{MAX}/P_{FAIL}) and corresponding shortenings ($\delta_{MAX}/\delta_{FAIL}$) are also recorded for the reference curves. The results obtained by the authors confirm their previous results obtained for the angle ply system, characterized by relatively high buckling load, low load capacity and curves close to the isotropic structures characterized by plastic flow. Interestingly, the effect of bending of analogous profiles made of GFRP is a permanent deformation of the structure after unloading, indicating the presence of permanent strains [53]. A similar phenomenon was neither observed within the framework of the research being the basis of this article nor in earlier works of authors referring to thinner channel section profiles made of GFRP [33].

Buckling modes and failure mechanisms recorded with the DIC system Aramis® for degraded and non-impacted channel-section profiles were included in Table 7. Analyzing the results presented in Table 7 it can be noticed that, in the case of initially degraded profiles, the number of the local buckling half-waves was not change in any of the cases studied. In opposition to impact analysis on flanges and webs of similar structures [32], the corner impact caused presence of the local unsymmetrical buckling mode which in turn is consistent with the results of tests carried out on similar material characterized by more than twice smaller thickness [33]. In all the analyzed cases, the collapse mechanism is created within the area of impact degradation ($L/2$), which in consequence also leads to an increase of the degradation area in relation to the postimpact state. In eight out of ten cases studied, the load capacity loss results from the stiffness loss on only one, impacted corner. In the case of the angle ply system impacted with energy of 20J at an angle of 45 and 90, however, it can be observed that the loss of load capacity is accompanied by the cracking of both corners located around the mid-span of the compressed columns. However, according to [32,33,53] one should not expect that a number of fracture points have a significant influence on the attained load carrying capacity.

Owing to a variety of parameters that can affect the stability, load carrying capacity and behavior of the profile in the pre- and postbuckling range, it was decided to compile the observed changes in a consolidated form in Table 8, which answers several key questions (A-H) in the context of the performed tests on predamaged thin-walled channel section composite profiles

In the light of the above-mentioned summary and in reference to the results of Gliszczynski et al. [32] and Kubiak et al. [33], it can be definitively concluded that the corner impact has an unambiguously negative influence on the behavior of thin-walled composite profiles subjected to compression. In opposition to the impacts located on the web or the flanges of similar C-shaped columns [32], corner impacts significantly reduce the load carrying capacity and cause asymmetrical local buckling modes. Degraded corners are the places of the collapse mechanism initiation during the CAI test. The direct consequence of this phenomenon is the increase in the area of projected damages compared to the postimpact state.

In conclusion, it should be highlighted that regardless of the scheme of the layers under consideration, the angular position of the impactor as well as the area and nature of the impact damages, all investigated cases were characterized by stable, postbuckling equilibrium paths. The natural effect of impact with higher energy was a larger damage area, which in turn led to the largest reduction in load carrying capacity during compression. However, in the context of the conducted studies, the unexpected result turned out to be a case of impact introduced perpendicular to the web of the channel section

Table 7
Buckling (B.M) and collapse modes (C.M.) for impacted and non-impacted channel section profiles.

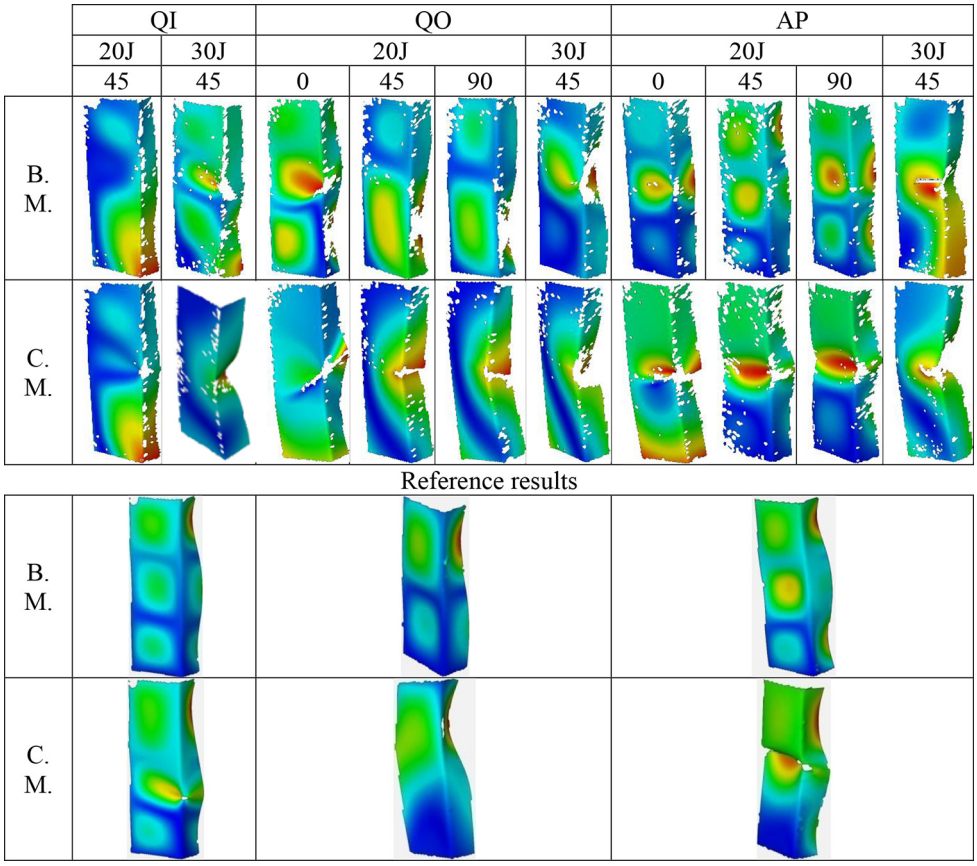

Table 8
Summary of conducted CAI tests.

A – What is the major type of impact damage?
B – How the buckling load change?
C – How the buckling mode change?
D – How the stiffness in the pre-buckling range change?
E – How the load carrying capacity change?
F – Is the failure mechanism initiated in the impact location?
G – Does the failure mechanism propagate through the initial damage area?
H – Does the damage area increase after CAI?

Ply system	Impact energy	Impact angle	A	B	C	D	E	F	G	H
QI	20 J	45	BVID	–	$_{-}^{UNS}$	–	↓↓↓	Y	Y	Y
	30 J	45	FR	–	$_{-}^{UNS}$	↓↓↓↓↓	↓↓↓↓	Y	Y	Y
QO	20 J	0	BVID	–	$_{-}^{UNS}$	–	↓↓	Y	Y	Y
		45	BVID	–	$_{-}^{UNS}$	–	↓↓↓	Y	Y	Y
		90	BVID/FR	–	$_{-}^{UNS}$	–	↓↓↓	Y	Y	Y
	30 J	45	FR	–	$_{-}^{UNS}$	↓↓↓↓↓	↓↓↓↓↓	Y	Y	Y
AP	20 J	0	CRACK*	–	$_{-}^{UNS}$	–	↓	Y	Y	Y
		45	CL	–	$_{-}^{UNS}$	–	↓	Y	Y	Y
		90	CRACK	–	$_{-}^{UNS}$	–	↓↓↓↓	Y	Y	Y
	30 J	45	CL	–	$_{-}^{UNS}$	↓↓↓↓↓	↓↓↓↓↓	Y	Y	Y

Notations:

Relative increase/decrease in specific range:

– - <0% ÷ 10%)
↑/↓ - <10% ÷ 20%)
↑↑/↓↓ - <20% ÷ 30%)
↑↑↑/↓↓↓ - <30% ÷ 40%)
↑↑↑↑/↓↓↓↓ - <40% ÷ 50%)
↑↑↑↑↑/↓↓↓↓↓ - <50% ÷ more)

Major type of damage
BVID – barely visible impact damage
FR - extensive fiber rupture
CL - continuity loss
CRACK – visible crack

Buckling half-waves
↗ - increase
– - no change
↘ - decrease
UNS - unsymmetrical

Answer
Y – yes
N - no

profiles (90). First, the nature of the initiated damages for both the quasi-isotropic (BVID/FT) and quasi-orthotropic (CRACK*) systems reached an intermediate damage pattern between what was observed for the other angular positions of the impactor (20J and 30J). Secondly, the examined cases with a 20J impact were not characterized by significant differences in the prebuckling stiffness. Although the final validation of these statements requires a much larger number of experimental tests, in the broader context this observation is crucial. If we assume that a structural plate system made of an analogous material would undergo impact event, characterized by the initiation of a similar pattern of internal damage, then the preliminary compression test (far below the buckling load) could not show significant differences in the stiffness and the global response understood as the course of the load vs shortening curve with respect to reference structures (contrary to the case of damage generated by energy 30J - stiffness from the very beginning of the compression test is different). In this case, when the impact damage would not be noticed, the process of applying the load from presumed safety region (from limit to ultimate load [54]) could result in an unexpected disaster. On the other hand, if we consider a method of joining thin-walled profiles (acting as stringer) to thin-walled composite shells (e.g. fuselage) [55,56], the described impact case seems highly unlikely because even if a C-profile is used, rather a flange than a web would be connected to the skin and exposed to impact event.

In the context of the considered ply systems, it should be mentioned that the quasi-isotropic system was characterized by the highest stiffness in the impact event, while during compression tests the quasi-orthotropic had highest stiffness in both, pre- and post-buckling range. Although the case of the quasi-isotropic system was not characterized by significant differences in relation to the reference response (force-shortening curve), the presence of additional longitudinal delamination outside the predefined impact area (limited by the inserts and clamping elements) is for the authors a motivation to continue the improvement of the proposed test stand for impact test of thin walled profiles.

6. Conclusions

Within the present study, experimental investigations of composite channel-section profiles subjected to corner impact and compression after impact were conducted. Different impact energies (20J, 30J) and corner impact angles (0, 45, 90) were analyzed. The structures under consideration were made of a GFRP laminate with quasi-isotropic, quasi-orthotropic and angle-ply arrangements of layers. The experimental results were compared to reference (not impacted) structures and to the literature results in which impacts in the middle of the web and flange width at different location in relation to the length of the profile were considered [32]. Based on the performed experimental studies it has been concluded that:

– in relation to Impact:
- no or nearly no relaxation in all corner impact cases prevents the use of a standard approach to damage qualifications within the limits of the applicability of the BVID definition;
- all analyzed cases were characterized by a high level of absorbed energy (over 75%), which led to the following damage: barely visible impact damage, extensive fiber rupture, visible laminate cracks or material continuity loss;
- the quasi-isotropic system was characterized by the highest stiffness and the impact force. No constant tendency between the impact angle and the maximum force can be derived;
- 45 degree impacts are characterized by the highest energy absorption, the largest registered indentation and simultaneously the relatively smallest area of damage in relation to other considered impact angles (0, 90);
- with regard to the 20 J impacts, the 90 degree position led to largest damage areas;
- quasi-orthotropic layup leads to the largest, quasi-isotropic to lowest damage area;
- the use of a portable gas gun impact device requires a strong data filtering algorithm;

– in relation to Compression After Impact:
  - all investigated cases were characterized by stable, postbuckling equilibrium paths;
  - the load carrying capacity of the profiles degraded by the corner impact always decreases in relation to the not-impacted structures;
  - the most dangerous 20 J impact scenario was the impact perpendicular to the web – 90 (characteristic features: no change in prebuckling stiffness in relation to reference structures, the highest load carrying capacity reduction compared to the other impact positions, continuous load carrying capacity loss – similar to the formation of plastic mechanisms in isotropic structures);
  - impacts with 20 J energy do not lead to significant stiffness differences in the prebuckling range (below 8%);
  - impacts with 30 J energy lead to a crucial decrease of the stiffness in the prebuckling state (over 60%) and cause the highest reduction in load capacity (at 50% compared to reference structures);
  - in all analyzed cases the failure mechanism is initiated in the impact location which leads to an increase of the damage areas during compression compared to the postimpact state;
  - the corner impacts caused an unsymmetrical local buckling mode.

The author's previous research assumed a scenario of impact and then compression [32,33], which may reflect the case of introducing damage after the end of the manufacturing process but before any assembly of the structural element and application of loads. In the future, the authors want to extend the research to the scenarios of impact on structures preloaded below the buckling load.

CRediT authorship contribution statement

A. Gliszczynski: Conceptualization, Data curation, Formal analysis, Funding acquisition, Investigation, Methodology, Project administration, Resources, Validation, Visualization, Writing - original draft. **R. Bogenfeld:** Data curation, Formal analysis, Investigation, Methodology, Validation, Visualization, Writing - original draft. **R. Degenhardt:** Supervision, Writing - review & editing. **T. Kubiak:** Conceptualization, Resources, Supervision.

Declaration of Competing Interest

The authors declare that they have no known competing financial interests or personal relationships that could have appeared to influence the work reported in this paper.

Acknowledgements

The investigations were conducted under projects UMO-2017/24/T/ST8/00483 and UMO-2016/23/N/ST8/01558. The first author would like to thank the Polish National Agency for Academic Exchange for financing the scientific internship under the Wilhelmina Iwanowska program at DLR.

Data availability

The raw/processed data required to reproduce these findings cannot be shared at this time as the data also forms part of an ongoing study.

Appendix A. Supplementary data

Supplementary data to this article can be found online at https://doi.org/10.1016/j.compstruct.2020.112502.

References

[1] Degenhardt R, Rolfes R, Zimmermann R, Rohwer K. COCOMAT - improved material exploitation of composite airframe structures by accurate simulation of postbuckling and collapse. Compos Struct 2006;73:175–8.
[2] Roskowicz M, Smal T. Research on durability of composite materials used in repairing aircraft components. Mainten Reliab 2013;15(4):349–55.
[3] Rana S, Fangueiro R. Advanced composite materials for aerospace engineering processing, properties and applications. Elsevier; 2016.
[4] Ishikawa T, Amaoka K, Masubuchi Y, Yamamoto T, Yamanaka A, Arai M, et al. Overview of automotive structural composites technology developments in Japan. Compos Sci Technol 2018;155:221–46.
[5] Chroscielewski J, Miskiewicz M, Pyrzowski L, Sobczyk B, Wilde K. A novel sandwich footbridge - practical application of laminated composites in bridge design and in situ measurements of static response. Compos Part B Eng 2017;126:153–61.
[6] Klasztorny M, Zajac KP, Nycz DB. GFRP composite footbridge series with multi-box cross section – part 1: design methodology, conceptual design and global detailed design. Compos Struct 2020;238:111965.
[7] Safri SNA, Sultan MTH, Yidris N, Mustapha F. Low velocity and high velocity impact test on composite materials – a review. Int J Eng Sci 2014;3(9):50–60.
[8] Richardson MOW, Wisheart MJ. Review of low-velocity impact properties of composite materials. Compos A Appl Sci Manuf 1996;27(12):1123–31.
[9] Boumbimba RM, Froustey C, Viot P, Gerard P. Low velocity impact response and damage of laminate composite glass fibre/epoxy based tri-block copolymer. Compos B Eng 2015;76:332–42.
[10] Bogenfeld R, Kreikemeier J, Wille T. Review and benchmark study on the analysis of low-velocity impact on composite laminates. Eng Fail Anal 2018;86:72–99.
[11] Wysmulski P, Debski H, Falkowicz K, Rozylo P. The influence of load eccentricity on the behavior of thin-walled compressed composite structures. Compos Struct 2019;213:98–107.
[12] Debski H, Rozylo P, Teter A. Buckling and limit states of thin-walled composite columns under eccentric load. Thin-Walled Struct 2020;149:106627.
[13] Czechowski L, Kedziora S, Kolakowski Z. The buckling and post-buckling of steel C-Columns in elevated temperature. Materials 2020;13(1):74.
[14] Czechowski L, Kolakowski Z. The study of buckling and post-buckling of a step-variable FGM box. Materials 2019;16(6):918.
[15] ASTM, 2015. Standard Test Method for Measuring the Damage Resistance of a Fiber-Reinforced Polymer Matrix Composite to a Drop-Weight Impact Event. Tech. rep., American Society for Testing and Materials (ASTM), West Conshohocken, PA, USA, ASTM D 7136/D 7136M-15.
[16] ASTM, 2012. Standard Test Method for Compressive Residual Strength Properties of Damaged Polymer Matrix Composite Plates. Tech. rep., American Society for Testing and Materials (ASTM), West Conshohocken, PA, USA, ASTM D7137/D7137M−12.
[17] Tuo H, Lu Z, Ma X, Zhang Ch, Chen Z. An experimental and numerical investigation on low-velocity impact damage and compression-after-impact behavior of composite laminates. Compos B Eng 2019;167:329–41.
[18] Ismail KI, Sultan MTH, Shah AUM, Jawaid M, Safri SNA. Low velocity impact and compression after impact properties of hybrid bio-composites modified with multi-walled carbon nanotubes. Compos B Eng 2019;163:455–63.
[19] Tan W, Falzon BG, Chiu LNS, Price M. Predicting low velocity impact damage and Compression-After-Impact (CAI) behaviour of composite laminates. Compos A 2015;71:212–26.
[20] Thorsson SI, Waas AM, Rassaian M. Low-velocity impact predictions of composite laminates using a continuum shell based modeling approach Part b: BVID impact and compression after impact. Int J Solids Struct 2018;155:201–12.
[21] Baykasoglu C, Baykasoglu A, Cetin MT. A comparative study on crashworthiness of thin-walled tubes with functionally graded thickness under oblique impact loadings. Int J od Crashworthiness 2019;24(4):453–71.
[22] Zhao Z, Zhu G, Zhou Ch, Yu Q. Crashworthiness analysis and design of composite tapered tubes under multiple load cases. Compos Struct 2019;222:110920.
[23] Ferdynus M, Kotełko M, Kral J. Energy absorption capability numerical analysis of thin-walled prismatic tubes with corner dents under axial impact. Maintenance Reliab 2018;20(2):252–9.
[24] Tanlak N, Sonmez FO. Optimal shape design of thin-walled tubes under high-velocity axial impact loads. Thin-Walled Struct 2014;84:302–12.
[25] Li N, Chen PH. Experimental investigation on edge impact damage and Compression-After-Impact (CAI) behavior of stiffened composite panels. Compos Struct 2016;138:134–50.
[26] Greenhalgh E, Meeks Ch, Clarke A, Thatcher J. The effect of defects on the performance of post-buckled CFRP stringer-stiffened panels. Composites: Part A 2003;34:623–33.
[27] Greenhalgh E, Clarke A, Thatcher J. Mechanical evaluation of stringer-stiffened panels tested under compression. Report: DERA.T3.TR.4. Farnborough (UK); 2000.
[28] Kootte LJ, Bisagni C. A Methodology to Investigate Skin-Stringer Separation in Postbuckled Composite Stiffened Panels, AIAA 2020-0477.
[29] Dávila CG, Bisagni C. Fatigue life and damage tolerance of postbuckled composite stiffened structures with indentation damage. J Compos Mater 2018;52(7):931–43.
[30] Wang XM, Cao W, Deng CH, Wang PY, Yue ZF. Experimental and numerical analysis for the post-buckling behavior of stiffened composite panels with impact damage. Compos Struct 2015;133:840–6.
[31] Kubiak T, Borkowski L, Wiacek N. Experimental investigations of impact damage influence on behavior of thin-walled composite beam subjected to pure bending. Materials 2019;12(7):1127.

[32] Gliszczynski A, Kubiak T, Borkowski L. Experimental investigation of pre-damaged thin-walled channel section column subjected to compression. Composites B 2018;147:56–68.
[33] Kubiak T, Gliszczynski A, Krygier M. Impact damage tolerance of laminate short columns subjected to uniform compression – experimental investigation. Compos Struct 2019;226:111222.
[34] Gliszczynski A, Kubiak T, Rozylo P, Jakubczak P, Bienias J. The response of laminated composite plates and profiles under low-velocity impact load. Compos Struct 2019;207:1–12.
[35] Abramovich H. Stability and Vibrations of Thin-Walled Composite Structures. Woodhead Publishing; 2017.
[36] Kubiak T. Static and dynamic buckling of thin-walled plate structures. Springer; 2013.
[37] ASTM D3039 / D3039M-17, Standard Test Method for Tensile Properties of Polymer Matrix Composite Materials, ASTM International, West Conshohocken, PA, 2017.
[38] ASTM D3410 / D3410M-16, Standard Test Method for Compressive Properties of Polymer Matrix Composite Materials with Unsupported Gage Section by Shear Loading, ASTM International, West Conshohocken, PA, 2016.
[39] Savitzky A, Golay MJE. Smoothing and differentiation of data by simplified least squares procedures. Anal Chem 1964;36(8):1627–39.
[40] Butterworth S. On the theory of filter amplifiers. Exp Wireless Wireless Eng 1930;7 (6):536–41.
[41] Wilson P. Design recipes for FPGAs using Verilog and VHDL. Newnes; 2016. p. 117–34.
[42] Urbaniak M, Teter A, Kubiak T. Influence of boundary conditions on the critical and failure load in the GFPR channel cross-section columns subjected to compression. Compos Struct 2015;134:199–208.
[43] Liu D, Lansing E, Malvern LE. Cracking in impacted glass/epoxy plates. J Compos Mater 1987;21:594–609.
[44] Liu D. Impact-induced delamination-a view of bending stiffness mismatching. J Compos Mater 1988;22:674–92.
[45] Song Z, Le J, Whisler D, Kim H. Skin-stringer interface failure investigation of stringer-stiffened curved composite panels under hail ice impact. Int J Impact Eng 2018;122:439–50.
[46] Polimeno U, Meo M. Detecting barely visible impact damage detection on aircraft composites structures. Compos Struct 2009;91:398–402.
[47] Shen Z, Tong X, Yang N, Xie M, Li Y, Chen P. Composite structure design and analysis. In: Yi XS, Du S, Zhang L, editors. Composite Materials Engineering, vol 1. Singapore: Springer; 2018.
[48] Galos J. Thin-ply composite laminates: a review. Compos Struct 2020;236 111920.
[49] Arteiro A, Furtado C, Catalanotti G, Linde P, Camanho PP. Thin-ply polymer composite materials: a review, Composites Part A: Applied Science and Manufacturing 2020;105777.
[50] Silberschmidt VV. Dynamic deformation, damage and fracture in composite materials and structures. Great Britain: Woodhead Publishing; 2016.
[51] Abrate S. Impact on composite structures. Cambridge University Press; 1998.
[52] Kim EH, Rim MS, Lee I, Hwang TK. Composite damage model based on continuum damage mechanics and low velocity impact analysis of composite plates. Compos Struct 2013;95:123–34.
[53] Jakubczak P, Gliszczynski A, Bienias J, Majerski K, Kubiak T. Collapse of channel section composite profile subjected to bending Part II: failure analysis. Compos Struct 2017;179:1–20.
[54] Wiedemann M, Sinapius M. Adaptive, Tolerant and Efficient Composite Structures, Springer, 2013.
[55] Bertolini J, Castanié B, Barrau JJ, Navarro JP, Petiot C. Multi-level experimental and numerical analysis of composite stiffener debonding. Part 2: element and panel level. Compos Struct 2009;90:392–403.
[56] Mittelstedt Ch, Schröder K-U. Local postbuckling of hat-stringer-stiffened composite laminated plates under transverse compression. Compos Struct 2010;92:2830–44.